

# Porous Materials Prepared by Sintering Basalt Fiber with CuS and ZrO<sub>2</sub> Additions and Containing a Rigid System of Microfiltration Transport Pores

S. M. Azarov<sup>a,\*</sup>, E. E. Petyushik<sup>b</sup>, E. M. Shishonok<sup>a</sup>, S. V. Zlotskii<sup>c</sup>, A.A Drobysh<sup>a</sup>, and A. V. Drozd<sup>b</sup>

<sup>a</sup> *Belarussian National Technical University, Minsk, 220013 Belarus*

<sup>b</sup> *State Research and Production Powder Metallurgy Association, Minsk, 220005 Belarus*

<sup>c</sup> *Belarussian State University, Minsk 220030, Belarus*

\*e-mail: [azarov@bntu.by](mailto:azarov@bntu.by)

Received December 14, 2022; revised April 5, 2023; accepted May 3, 2023

**Abstract**—Porous ceramic materials have been prepared from BS16-6-76 chopped basalt fiber with CuS and ZrO<sub>2</sub> additions by granulation, pressing, and subsequent sintering in air. Computer-controlled X-ray diffraction measurements have been used to carry out profile analysis and assess the qualitative and relative quantitative phase compositions of the materials. We have identified the sequence of phase transformations in the basalt fiber and confirmed that fiber crystallization during cooling after sintering begins with the formation of aluminosilicate spinel nuclei, which act as crystallization centers and become incorporated into the structure of orthoclase. The last to form in the phase hierarchy is a low-molecular-weight Fe-containing phase, namely, hematite ( $\alpha$ -Fe<sub>2</sub>O<sub>3</sub>), built in a framework silicate of isomorphous series. The surface of the basalt fiber in the sintered material modified with copper sulfide and zirconium oxide additions has been shown to be covered with ~500-nm inclusions of a crystalline phase.

**Keywords:** basalt, fiber, iron oxides, aluminosilicates, structure, phase composition

**DOI:** 10.1134/S002016852306002X

## INTRODUCTION

The potential of ceramic fiber-based porous materials for use in catalytic cracking and internal combustion engine exhaust purification systems is determined by their high-temperature service conditions, with their technological strength retained. Interest in the use of basalt fiber for catalytic reactions in gas flows is aroused by the possibility of producing a porous fibrous matrix having a rigid system of microfiltration pores and high air permeability. Azarov [1] and Petyushik et al. [2] studied distinctive features of structure formation in porous materials prepared by sintering basalt fiber and examined the influence of shaping and heat treatment conditions and properties of the starting mixture on characteristics of experimental samples. The range of characteristics of the resultant materials was rather wide: their pore size ranged from 2.7 to 16  $\mu\text{m}$ ; their compressive strength, from 0.2 to 2.1 MPa; and their air permeability, from  $2 \times 10^{-10}$  to  $9 \times 10^{-10}$  m<sup>2</sup>. Recent work [3, 4] has shown that porous materials prepared by sintering basalt fiber retained its technological strength upon additional heat treatment after sintering and subsequent sharp cooling in various media.

At present, on the order of 75% of all reactions in oil refining processes are catalytic. Industrial catalysts

that are used in such processes have the form of one-, two- three-, or four-component systems based on nonferrous metal oxides [5]. The presence of sulfur in catalysts had long been thought to have a negative effect on the rate of any reactions that occur on the surface of catalysts. However, studies of well-known sulfides [6] showed that some sulfur compounds, including copper sulfide, CuS, exhibit catalytic properties [7].

The purpose of this work was to study the phase composition of porous materials having a rigid system of microfiltration transport pores and produced by sintering basalt fiber with additions of sulfur and zirconium compounds for use in catalytic treatment of gas flows.

## EXPERIMENTAL

We studied samples of porous materials (hereafter simply samples) 17 mm in diameter and 5–17 mm in thickness, which were prepared by sintering basalt fiber with zirconium oxide and/or copper sulfide additions in air at 1075°C under previously described conditions [1]. The appearance of the samples and the structure of the porous material are shown in Fig. 1.

The strength, density, porosity, specific surface area, and phase composition of the samples were

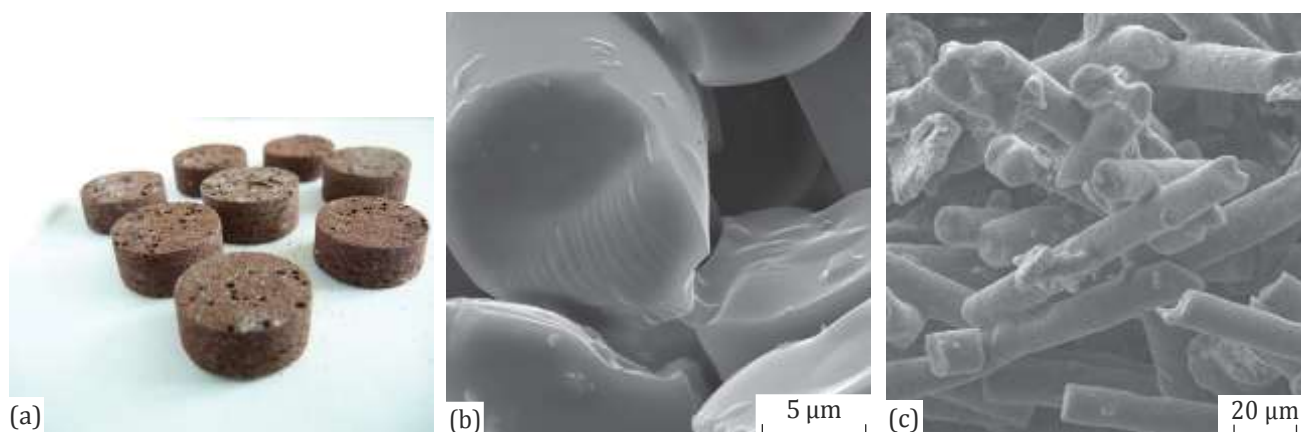


Fig. 1. Basalt fiber samples (a) and structure of the basalt fiber (b) and fiber-based material.

determined by standard techniques commonly used in materials research. The phase composition of the materials was determined by X-ray diffraction on a Rigaku Ultima IV diffractometer in parallel beam geometry with  $\text{CuK}\alpha$  radiation (wavelength of 0.154179 nm). We used PDXL 2 software, supplied with the diffractometer, to perform profile analysis of X-ray diffraction patterns, determine qualitative and relative quantitative (Table 1) phase compositions of our samples, carry out structural analysis, and calculate lattice parameters of the phases present, as a standard approach, in particular, used by Shishonok et al. [8].

Both the as-prepared samples, represented in Fig. 1a, and powders prepared by grinding them (hereafter powder materials) were characterized by X-ray diffraction. Survey X-ray diffraction patterns were collected by a standard technique in the angular range  $0^\circ$ – $100^\circ$  in continuous scan mode at a rate of  $2^\circ/\text{min}$  or at a scan step of  $0.05^\circ$ .

### RESULTS AND DISCUSSION

The X-ray diffraction patterns shown in Fig. 2 represent different structural and phase states of two types of powder materials, containing different additions. We call attention to the stronger halo in the range  $2\theta \sim 20^\circ$ – $40^\circ$ , with an angular width  $\Delta \sim 20^\circ$ , and a broader

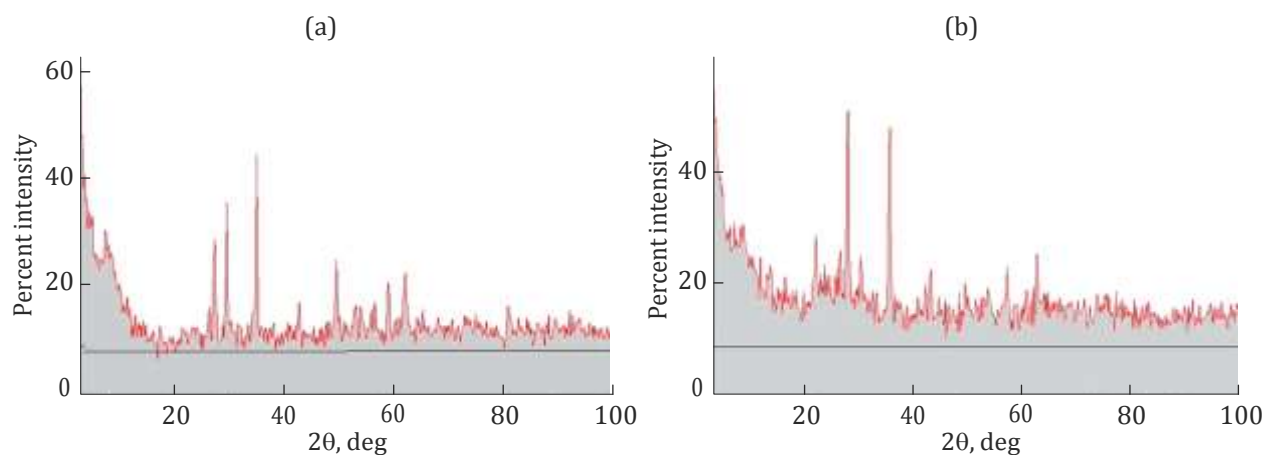
range of increased intensity at small angles  $2\theta \sim 0^\circ$ – $20^\circ$  in Fig. 2b in comparison with Fig. 2a. Moreover, the X-ray diffraction pattern in Fig. 2b has a stronger background. We can compare intensities in Figs. 2a and 2b because the X-ray diffraction patterns were collected under identical conditions.

It is known [9] that an amorphous phase in the composition of any material leads to the presence of a halo, typically at least  $\Delta(2\theta) \sim 20^\circ$  in width, in any angular range of its X-ray diffraction pattern. The X-ray diffraction pattern then has a rather high overall background, which is a consequence of scattering by disordered regions in the structure of the material. Fully amorphous materials have no sharp reflections [10]. On the other hand, complete crystallization of an amorphous phase leads to a sharp drop in the intensity of the halo and background and simultaneous formation of sharp reflections from the crystalline phase. Clearly, partial crystallization leads to partial changes in the intensity of the background and halo and the formation of sharp reflections with a varying full width at half maximum.

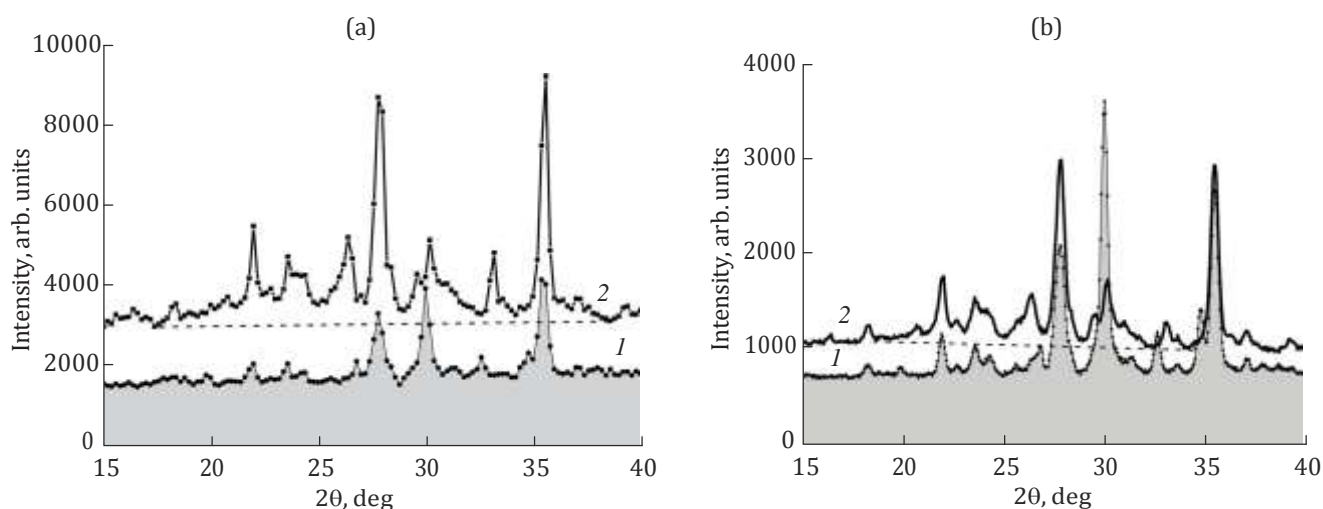
It is clear from the above considerations that, from the viewpoint of its structure, the powder material containing CuS additions is a partially amorphous material, but it has a higher amorphous content than does the powder material containing both CuS and

Table 1. Phase composition of materials prepared by sintering basalt fiber at  $1075^\circ\text{C}$  (relative amounts of phases estimated using Rigaku PDXL 2 software)

C, arb. units										
Copper sulfide and zirconium oxide additions										
$\text{CaAl}_2\text{Si}_2\text{O}_8$	$\text{Al}_2\text{O}_3$	$\text{Fe}_3\text{O}_4$	$\text{K}_2\text{O}$	$\text{CuS}$	$\text{MgO}$	$\text{TiO}_2$	$\text{CaO}$	$\text{Na}_2\text{O}$	$\text{ZrO}_2$	$\text{SiO}_2$
1.57	1.665	<b>1.026 (~6%)</b>	1.4	1.49	0.976	1.24	2.819	2.607	1.37	1.101
Copper sulfide additions										
2.086	2.114	<b>0.663 (~4%)</b>	1.817	2.026	1.424	1.642	1.687	2.986		1.23



**Fig. 2.** X-ray diffraction patterns of the powder materials containing (a) CuS + ZrO<sub>2</sub> and (b) CuS additions (identical sample weights and X-ray diffraction pattern collection conditions in both cases).



**Fig. 3.** X-ray diffraction patterns of the (a) powder materials and (b) samples in the range 15°–40°: (1) CuS + ZrO<sub>2</sub> additions, (2) CuS additions.

ZrO<sub>2</sub> additions. A second overall phase in both materials is a crystalline phase—several phases in our case, which are evidenced by strong, sharp lines. According to results for the unmilled ceramic materials, the full width at half maximum (FWHM) of the sharp reflections from them was  $\sim 0.06^\circ$ – $0.5^\circ$  (as determined by profile analysis), and these reflections were used to determine the phase composition of the materials we obtained.

The increased intensity of the halo in the angular range  $2\theta \sim 0^\circ$ – $20^\circ$  in both X-ray diffraction patterns and the higher halo intensity in Fig. 2b are a consequence of X-ray scattering by small inhomogeneities having no ordered structure, which are more abundant in the powder material containing CuS additions.

For comparison, Fig. 3 presents X-ray diffraction patterns of the powders (Fig. 3a) and the porous materials from which the powders were prepared (Fig. 3b).

The data were collected in the range  $2\theta = 15^\circ$ – $40^\circ$  at a scan rate of  $0.1^\circ/\text{min}$  with a scan step of  $0.2^\circ$ . It is seen that, for both the samples and powders, the halo is broader in the case of CuS additions than in the case of CuS + ZrO<sub>2</sub> additions. Note that the difference in width is larger in the case of the powder materials, the data for which were collected under nearly classical conditions.

Figure 4 shows X-ray diffraction patterns of the samples containing CuS + ZrO<sub>2</sub> (scan 1) and CuS (scan 2) additions in the angular ranges  $10^\circ$ – $120^\circ$  and  $15^\circ$ – $65^\circ$ . Clearly, the sample prepared by sintering with CuS additions (Fig. 4a, scan 2) contains a smaller amount of the amorphous phase before milling than after (Fig. 3a, scan 2), as evidenced by the fact that, in the former case, the halo is located in a narrower angular range. Since the background in the X-ray diffrac-

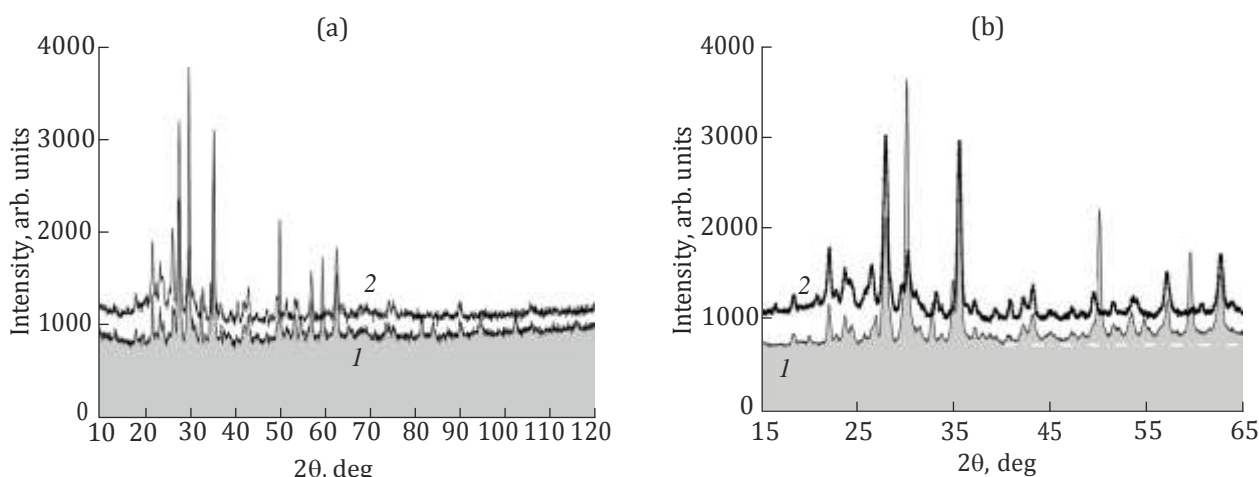


**Fig. 4.** X-ray diffraction patterns of the samples in the angular ranges (a) 10°–120° and (b) 15°–65°: (1) CuS + ZrO<sub>2</sub> additions, (2) CuS additions.

tion pattern of the materials containing CuS + ZrO<sub>2</sub> additions is weaker, the amount of inhomogeneities and structural imperfections is on the whole smaller in this material.

Another characteristic feature in the behavior of the background in the X-ray diffraction patterns can be seen in Figs. 4a and 4b: the background intensity increases with increasing 2θ angle and the increase is larger for the material containing CuS + ZrO<sub>2</sub> additions (scans 1). It is known that such behavior can be caused by fluorescence of Fe atoms and is characteristic of samples containing an Fe compound. Judging from scans 1, the amount of this compound, relatively small, is larger in the material containing CuS + ZrO<sub>2</sub> additions. This conclusion is well confirmed by the fact that the X-ray diffraction patterns were obtained using CuK<sub>α</sub> radiation and, in this case, fluorescence would be expected for Fe and Co atoms [11]. The presence of cobalt in the materials is unlikely. It follows from the data in Table 1, which presents the phase composition of the materials and the relative amounts of phases estimated using Rigaku PDXL 2 software, and relatively simple mathematical calculations that the relative amount of Fe<sub>2</sub>O<sub>3</sub> is a factor of 1.5 larger in the material containing CuS + ZrO<sub>2</sub> additions than in the material containing only CuS additions.

It is known that, unlike in the case of basalt, whose major mineralogical components are aluminosilicates, the major components of basalt fiber are SiO<sub>2</sub>, Al<sub>2</sub>O<sub>3</sub>, CaO, and others [12]. It follows from Table 1 that the number of the phases identified in the materials obtained in this study is at least 11, including Fe<sub>3</sub>O<sub>4</sub>, Fe<sub>2</sub>O<sub>3</sub>, ZrO<sub>2</sub>, and CuS.

The phase composition of the materials prepared by sintering basalt fiber with CuS + ZrO<sub>2</sub> or CuS additions was estimated to a depth of 80 μm at a diffraction angle of 30°.

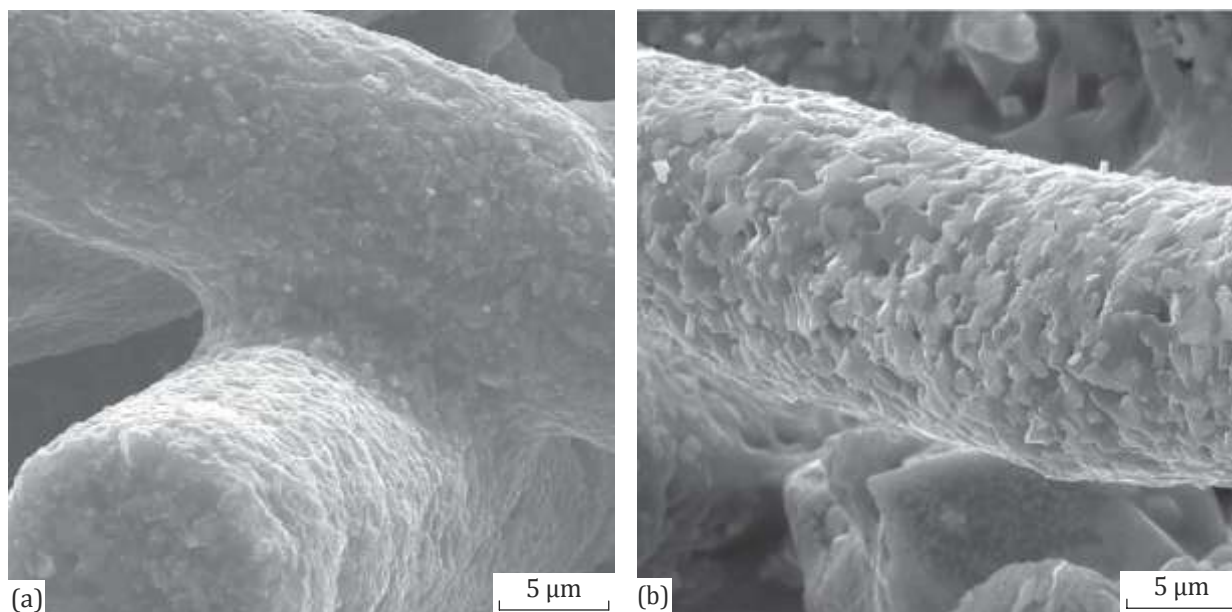
In analyzing the data in Table 2, with allowance for the structure of the porous material (Fig. 1c), it is reasonable to assume that the pores in it are essentially open. Taking the average density of basalt to be ~3 g/cm<sup>3</sup>, we obtain that the calculated porosity of our samples is 50–80%.

Figure 5 illustrates the surface microstructure of the basalt fiber in the composition of the samples containing CuS and CuS + ZrO<sub>2</sub> additions. X-ray microanalysis data for the elements Si, Cu, Fe, O, S, Ca, Al, and Zr along segment AB (Fig. 6, inset) on the fiber surface in the material containing CuS + ZrO<sub>2</sub> additions confirm the presence of the phases listed in Table 1.

It is known that the major mineralogical components of basalt are aluminosilicates—minerals of the

**Table 2.** Properties of the samples prepared by sintering at 1075°C

Compressive strength, MPa	Density, g/cm <sup>3</sup>	Specific surface area, m <sup>2</sup> /g	Percent porosity
Copper sulfide additions			
2.0–2.2	0.8–0.85	0.237–0.376	47–57
Copper sulfide + zirconium oxide additions			
1.9–2.7	0.91–0.93	0.467–0.654	49–54



**Fig. 5.** Surface microstructure of the basalt fiber in the composition of the samples containing (a) CuS and (b) CuS + ZrO<sub>2</sub> additions.

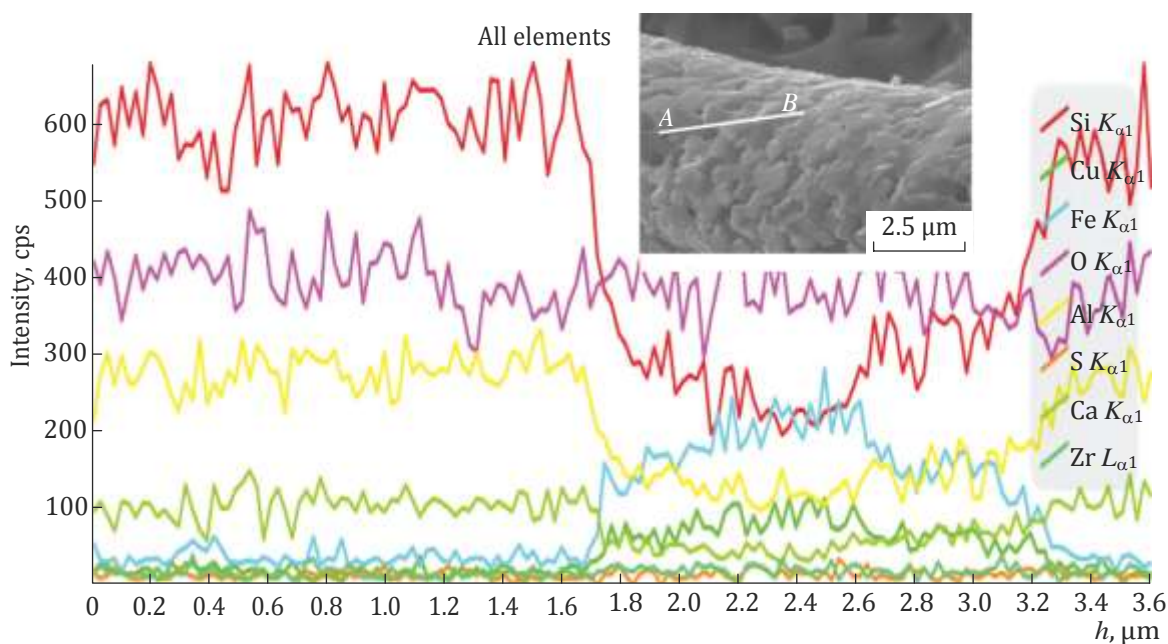


**Fig. 6.** X-ray microanalysis data for the elements Si, Cu, Fe, O, S, Ca, Al, and Zr on the surface of the sample containing copper sulfide and zirconium oxide additions (inset: image of the zone studied along segment *AB*).

pyroxene and plagioclase groups consisting of solid solutions of variable composition. Iron oxides are present predominantly in magnetite, andradite, and other minerals [13]. As shown earlier [14–17], heating basalt fiber to above 1000°C leads to destruction of chain silicate structures, accompanied by the formation of hematite (low-molecular-weight Fe-contain-

ing phase,  $\alpha$ -Fe<sub>2</sub>O<sub>3</sub>) and a framework silicate of iso-morphous series.

At the same time, according to Kruchinin and Belousov [16] heating to above 1000°C leads to a reduction in the viscosity of the amorphous fiber matrix. The crystallization energies calculated by Manylov et al. [17] for spinel, pyroxene, and plagioclase phases

suggest that the most likely result of cooling is the formation of a spinel phase. This, in turn, points to three- and two-dimensional crystal growth at a constant number of nuclei [18].

Thus, the first step in fiber crystallization during cooling is the formation of potassium aluminosilicate nuclei, which act as crystallization centers and become incorporated into the structure of orthoclase. The last to form in the phase hierarchy is a low-molecular-weight Fe-containing phase built in a framework silicate of isomorphous series.

The above assumptions are supported by images of the surface structure of the basalt fiber in the composition of the material of the sample prepared by sintering with additions of the sulfur and zirconium compounds (Fig. 6) and the X-ray microanalysis data for this material. It follows from the X-ray microanalysis data that the zone under study on the surface of basalt fiber contains regions ranging in size from ~100 to 500 nm and having increased iron, copper, and oxygen concentrations (which is indirect evidence for the presence of  $\text{Fe}_3\text{O}_4$  and CuS), in combination with a considerable decrease in silicon content and a slight decrease in aluminum content.

As emphasized by Augis and Bennett [19], the crystallization tendency of powdered iron-rich glasses is weaker in air because of the surface oxidation of  $\text{Fe}_2\text{O}_3$  to  $\text{Fe}_3\text{O}_4$ . The present results demonstrate that no surface oxidation of  $\text{Fe}_2\text{O}_3$  to  $\text{Fe}_3\text{O}_4$  occurs during sintering of basalt fiber containing copper sulfide additions (Table 1). Karamanov et al. [20] reported that there was no oxidation in a neutral atmosphere. Therefore, according to a mechanism described by Pukh et al. [21] crystallization on the surface of basalt fiber begins with the formation of magnetite ( $\text{Fe}_3\text{O}_4$ ) and covellite (CuS), following which the crystals act as anorthite ( $\text{CaAl}_2\text{Si}_2\text{O}_8$ ) formation centers. At the same time, the crystallization process, involving the formation of a combination of crystalline phases, namely, magnetite ( $\text{Fe}_3\text{O}_4$ ), covellite (CuS), and anorthite ( $\text{CaAl}_2\text{Si}_2\text{O}_8$ ), both inhibits the surface oxidation of  $\text{Fe}^{2+}$  to  $\text{Fe}^{3+}$  and creates conditions for the formation of a large number of crystals ~500 nm in size on the surface of the material (Fig. 5).

The differences in the surface morphology of basalt fiber between the samples containing CuS and CuS +  $\text{ZrO}_2$  additions (Fig. 5) determine the difference between their specific surface areas. The data presented in Table 2 demonstrate that the specific surface area of the samples sintered with copper sulfide and zirconium oxide additions is about twice that of the samples containing no zirconium oxide.

## CONCLUSIONS

According to the present results on the phase structure of porous materials having a rigid system of microfiltration transport pores and produced by sin-

tering basalt fiber with additions of zirconium oxide and/or a sulfur compound, the material modified with CuS +  $\text{ZrO}_2$  additions contains a much larger amount of a more homogeneous and structurally perfect crystalline phase in comparison with the material modified with CuS additions, which contains a relatively large amount of an amorphous phase.

The surface of the basalt fiber in the sintered material modified with copper sulfide and zirconium oxide additions has been shown to be covered with ~500-nm inclusions of a crystalline phase. The specific surface area of the material containing CuS +  $\text{ZrO}_2$  additions exceeds that of the material containing only CuS additions. The increase in the specific surface area of the porous material is potentially attractive for improving its catalytic activity.

We expect that the presence of iron(II, III) oxide ( $\text{Fe}_3\text{O}_4$ ) and transition metal sulfide (CuS) nano-inclusions in combination with the predominance of a crystalline phase in the samples modified with CuS +  $\text{ZrO}_2$  additions [5, 6] will ensure catalytic activity of the porous materials studied here, in particular for the alkylation of aromatic hydrocarbons and conversion of high-molecular-weight components of heavy crude oil in a carbonic acid solution.

## FUNDING

@@@@@@

## CONFLICT OF INTEREST

The authors declare that they have no conflicts of interest.

## REFERENCES

1. Azarov, S.M., Conditions for the formation of porous composite materials with enhanced strength from aluminosilicate powders and basalt fiber, part 1, *Poroshk. Metall.* (Minsk, Belarus), 2018, no. 41, pp. 90–94.
2. Petyushik, E.E., Azarov, S.M., Drobysh, A.A., Markova, L.V., and Gamzeleva, T.V., Structure and properties of porous composite materials based on aluminosilicate powders and basalt fiber, *Poroshk. Metall.* (Minsk, Belarus), 2018, no. 41, pp. 147–152.
3. Petyushik, E., Azarau, S., Azarava, T., Besarab, S., Drobysh, A., and Sauka, J., Investigation of the structure and properties of ceramic materials with a rigid system of microfiltration transport pores based on basalt fibers, *J. Metastable Nanocryst. Mater.*, 2022, vol. 34, pp. 13–18.
4. Vusikhis, A.S., Sergeeva, S.V., Gulyaeva, R.I., Ryabov, V.V., and Chentsov, V.P., Structure-sensitive properties of melts and thermal properties of glasses in the  $\text{B}_2\text{O}_3$ – $\text{CaO}$ – $\text{Al}_2\text{O}_3$ – $\text{PbO}$  system, *Inorg. Mater.*, 2022, vol. 58, no. 1, pp. 97–103. <https://doi.org/10.1134/S0020168522010149>
5. Khisamov, R.S., *Vysokoeffektivnye tekhnologii osvoeniya neftyanykh mestorozhdenii* (Highly Effective Technologies for Oil Field Development), Moscow: Nedra, 2004.

6. Tomina, N.N., Pimerzin, A.A., and Moiseev, I.K., Sulfide catalysts for the hydrotreating of crude oil fractions, *Ross. Khim. Zh.*, 2008, vol. 52, no. 4, pp. 41–52.
7. Kayukova, G.P., Feoktistov, D.A., Vakhin, A.V., Kosachev, I.P., Romanov, G.V., Mikhailova, A.N., and Khisamov, R.S., Conversion of heavy crude oil in a carbonic acid solution with the use of iron disulfide as a natural catalyst, *Neft. Khoz.*, 2017, no. 4, pp. 100–102. <https://doi.org/10.24887/0028-2448-2017-4-100-102>
8. Shishonok E.M., Steeds, J.W., Pysk A.V., Mosunov E.I., Abdullaev O.R., Yakunin A.S., and Zhigunov D.M., Structural study of rare-earth-doped cubic boron nitride micropowders, *Poroshk. Metall.*, 2011, no. 11/12, pp. 95–114.
9. Abrosimova, G.E., Aronin, A.S., and Kholstinina, N.N., On the determination of the volume fraction of the crystalline phase in amorphous–crystalline alloys, *Phys. Solid State*, 2010, vol. 52, no. 3, pp. 445–451.
10. Kovalev, D.Yu., Dynamic X-ray diffraction characterization of material-forming combustion processes, *Doctoral (Phys.–Math.) Dissertation*, Chernogolovka, 2021. <https://www.dissercat.com/content/dinamicheskaya-rentgenografiya-materialoobrazuyushchikh-protsessov-goreniya>. Accessed March 15, 2023.
11. Abyzov, A.M., *Rentgenodifraktsionnyi analiz polikristallicheskih veshchestv (X-Ray Diffraction Analysis of Polycrystalline Substances)*, St. Petersburg: SPbGTI (TU), 2008.
12. *Entsiklopediya neorganicheskikh materialov (Encyclopedia of Inorganic Materials)*, Kiev: Ukrainsk. Sov. Entsiklopediya, 1977, vol. 1.
13. Strelov, K.K., *Struktura i svoistva ogneporov (Structure and Properties of Refractories)*, Moscow: Metallurgiya, 1982.
14. Karamanov, A. and Pelino, M., Crystallization phenomena in iron-rich glasses, *J. Non-Cryst. Solids*, 2001, vol. 281, pp. 139–151. [https://doi.org/10.1016/S0022-3093\(00\)00436-1](https://doi.org/10.1016/S0022-3093(00)00436-1)
15. Dzhigiris, D.D. and Makhova, M.F., *Osnovy proizvodstva bazal'tovykh izdelii (Principles of the Production of Basalt Articles)*, Moscow: Teploenergetika, 2002.
16. Kruchinin, Yu.D. and Belousov, Yu.L., Formation of spinel phases in iron oxide-containing pyroxene glasses, *Fiz. Khim. Stekla*, 1976, vol. 2, no. 3, pp. 242–245.
17. Manylov, M.S., Gutnikov, S.I., Lipatov, Ya.V., Pokholok, K.V., Filimonov, D.S., and Lazoryak, B.I., Crystallization of continuous basalt fiber in an oxidizing atmosphere, *Fiz. Khim. Stekla*, 2012, vol. 38, no. 4, pp. 565–573.
18. Gutnikov, S.I., Manylov, M.S., Lipatov, Ya.V., Lazoryak, B.I., and Pokholok, K.V., Effect of the reduction treatment on the basalt continuous fiber crystallization properties, *J. Non-Cryst. Solids*, 2013, vol. 368, pp. 45–50. <https://doi.org/10.1016/j.jnoncrysol.2013.03.007>
19. Augis, J.A. and Bennett, J.E., Calculation of the Avrami parameters for heterogeneous solid state reactions using a modification of the Kissinger method, *J. Therm. Anal.*, 1978, vol. 13, pp. 283–292. <https://doi.org/10.1007/bf01912301>
20. Karamanov, A., Piscicella, P., and Pelino, M., The crystallisation kinetics of iron-rich glass in different atmospheres, *J. Eur. Ceram. Soc.*, 2000, vol. 20, pp. 2233–2237. [https://doi.org/10.1016/S0955-2219\(00\)00077-7](https://doi.org/10.1016/S0955-2219(00)00077-7)
21. Pukh, V.P., Baikova, L.G., Kireenko, M.F., Tikhonova, L.V., Kazannikova, T.P., and Sinani, A.B., Atomic structure and strength of inorganic glasses, *Phys. Solid State*, 2005, vol. 47, no. 5, pp. 876–881.

*Translated by O. Tsarev*

**Publisher's Note.** Pleiades Publishing remains neutral with regard to jurisdictional claims in published maps and institutional affiliations.

SPELL: 1. OK